AGU PUBLICATIONS
JGR
Journal of Geophysical Research: Space Physics

RESEARCH ARTICLE
10.1002/2016JA022496

Key Points:
- Parallel variances are robustly generated in compressible MHD turbulence, even when absent initially
- They are usually a minority of the fluctuation energy
- Perpendicular and parallel variances are not independent

Correspondence to:
S. Oughton,
seano@waikato.ac.nz

Citation:
Oughton, S., W. H. Matthaeus, M. Wan, and T. Parashar (2016), Variance anisotropy in compressible 3-D MHD, *J. Geophys. Res. Space Physics*, *121*, 5041–5054, doi:10.1002/2016JA022496.

Received 9 FEB 2016
Accepted 29 MAY 2016
Accepted article online 7 JUN 2016
Published online 28 JUN 2016

Variance anisotropy in compressible 3-D MHD

S. Oughton[1], W. H. Matthaeus[2], Minping Wan[3], and Tulasi Parashar[2]

[1]Department of Mathematics, University of Waikato, Hamilton, New Zealand, [2]Department of Physics and Astronomy, University of Delaware, Newark, Delaware, USA, [3]Department of Mechanics and Aerospace Engineering, South University of Science and Technology of China, Shenzhen, China

Abstract We employ spectral method numerical simulations to examine the dynamical development of anisotropy of the variance, or polarization, of the magnetic and velocity field in compressible magnetohydrodynamic (MHD) turbulence. Both variance anisotropy and spectral anisotropy emerge under influence of a large-scale mean magnetic field $\boldsymbol{B}_0$; these are distinct effects, although sometimes related. Here we examine the appearance of variance parallel to $\boldsymbol{B}_0$, when starting from a highly anisotropic state. The discussion is based on a turbulence theoretic approach rather than a wave perspective. We find that parallel variance emerges over several characteristic nonlinear times, often attaining a quasi-steady level that depends on plasma beta. Consistency with solar wind observations seems to occur when the initial state is dominated by quasi-two-dimensional fluctuations.

1. Introduction

A prominent feature of a magnetohydrodynamic (MHD) fluid or plasma under influence of a large-scale mean magnetic field is the appearance of two kinds of anisotropy, which we refer to as *variance* anisotropy and *spectral* anisotropy. The former type, which is the primary focus of the present paper, refers to the inequality of the diagonal elements of the variance tensor $V_{ij} = \langle B_i B_j \rangle - \langle B_i \rangle \langle B_j \rangle$, for the special case of the magnetic field vector $\boldsymbol{B}$, and is sometimes, in wave theory, called "polarization" anisotropy [*Coleman*, 1968; *Belcher and Davis Jr.*, 1971; *Barnes*, 1979]. Angle brackets denote an appropriate average. The second type, spectral anisotropy, may also be called correlation anisotropy and refers to the inequality of the total energy density $S_{ii}(\boldsymbol{k})$ (summed over all diagonal components of the spectral tensor S_{ij}) near wave vector $\boldsymbol{k}$ when the direction (only) of $\boldsymbol{k}$ is varied [*Batchelor*, 1970; *Robinson and Rusbridge*, 1971; *Shebalin et al.*, 1983].

In the present paper we will examine how variance anisotropy emerges in several contexts that are familiar in plasma and MHD turbulence. For example, we will begin by asking whether freely decaying (undriven) turbulence that begins with variances fully transverse to the applied mean magnetic field, $\boldsymbol{B}_0$, will remain in this state. Fluctuations that remain fully transverse are sometimes called "Alfvén modes" or "Alfvénic modes," referring to a linear wave perspective [*Barnes*, 1979], but, in general, they are not required to be associated with waves. When departures from the transverse variance condition are observed, we address the issues of how fast parallel variances appear and, in a quantitative sense, what levels of anisotropy are favored. Following a review of background (section 2) and a description of the numerical methods (section 3), we examine these questions in section 4, using results from simulations. This leads naturally to discussion of how variance anisotropy is related to other features such as Alfvén ratio (kinetic to magnetic energy ratio) and spectral anisotropy. Our attention then turns to results relating to the degree of independence of parallel and transverse variances. Finally, we discuss the implications of the present series of numerical experiments. We note that these same questions and issues have also been recently investigated in a companion kinetic plasma study [*Parashar et al.*, 2016].

2. Motivation and Theoretical Background

While the two kinds of anisotropy can be related (as we discuss below), from a purely kinematic perspective they are entirely independent. For example, in constructing a synthetic turbulence realization (where synthetic means that any correlations between field components have not been attained dynamically) one is free to choose a distribution of energy over wave vector, i.e., $S(\boldsymbol{k}) \equiv S_{ii}(\boldsymbol{k})$, and then after the fact choose how the variance is distributed. In fact, in a large periodic box, one can always represent the Fourier coefficients of the

magnetic field, $\boldsymbol{B}(\boldsymbol{x}) = \sum_{\boldsymbol{k}} \tilde{\boldsymbol{b}}(\boldsymbol{k}) e^{i\boldsymbol{k}\cdot\boldsymbol{x}}$, using the toroidal-poloidal (aka Craya-Herring) decomposition [*Craya*, 1958; *Herring*, 1974; *Lee*, 1975; *Lesieur*, 1990; *Howes*, 2015],

$$\tilde{\boldsymbol{b}}(\boldsymbol{k}) = \frac{i\boldsymbol{k}\times\hat{\boldsymbol{z}}}{k_\perp}\tilde{b}_t(\boldsymbol{k}) - \frac{\hat{\boldsymbol{k}}\times(\boldsymbol{k}\times\hat{\boldsymbol{z}})}{k_\perp}\tilde{b}_p(\boldsymbol{k}), \tag{1}$$

where $k_\perp = |\boldsymbol{k}\times\hat{\boldsymbol{z}}|$, $\hat{\boldsymbol{k}} \equiv \boldsymbol{k}/k$, and a uniform mean magnetic field $\boldsymbol{B}_0 = B_0\hat{\boldsymbol{z}}$ is in the $\hat{\boldsymbol{z}}$ direction. (When $\boldsymbol{k} \parallel \boldsymbol{B}_0$, we choose the toroidal and poloidal directions to be $\hat{\boldsymbol{x}}$ and $\hat{\boldsymbol{y}}$, respectively.) Then the energy distribution will be the selected value provided that $S(\boldsymbol{k}) = \langle|\tilde{b}_t(\boldsymbol{k})|^2 + |\tilde{b}_p(\boldsymbol{k})|^2\rangle$. We are still free to choose how this energy is partitioned between the toroidal component (aka Alfvénic polarization) $\tilde{b}_t(\boldsymbol{k})$ and the poloidal component $\tilde{b}_p(\boldsymbol{k})$, and this selection determines the degree of variance anisotropy with respect to the $\boldsymbol{B}_0$ direction, which is the main emphasis below. Spectral anisotropy is now imposed by selecting how the amplitudes are distributed over the *directions* of the wave vector $\boldsymbol{k}$. Polarization within the perpendicular plane is also affected by this choice. (For details and the full formulation of the spectral tensor, see, e.g., *Oughton et al.* [1997].)

Similarly, the velocity field $\boldsymbol{v}(\boldsymbol{x})$, which is not guaranteed to be solenoidal, consists of toroidal and poloidal contributions $\tilde{v}_p(\boldsymbol{k})$, $\tilde{v}_t(\boldsymbol{k})$ as above, but in addition may include a *longitudinal* part having Fourier amplitudes of the form $\tilde{\boldsymbol{u}}_L(\boldsymbol{k}) = \hat{\boldsymbol{k}}\tilde{u}_L(\boldsymbol{k})$.

In the solar wind, the classic examination of the variance anisotropy is due to *Belcher and Davis Jr.* [1971], which characterized the full range of possibilities in terms of the eigenvalues of the variance tensor. Analyzing Mariner data, they found the *minimum variance* direction to be located very close to the mean magnetic field direction and the variance ratios in the inertial range to be close to 5:4:1, which is consistent with statistical axisymmetry about the mean field [e.g., *Leamon et al.*, 1998]. This ratio implies that the perpendicular variance $\langle b_\perp^2\rangle = \langle b_x^2 + b_y^2\rangle$ exceeds the parallel variance $\langle b_z^2\rangle$ by a factor of about 9 for the interval analyzed. More extensive studies at MHD scales have shown that the solar wind typically has

$$A^b = \frac{\langle b_\perp^2\rangle}{\langle b_z^2\rangle} > 2 \tag{2}$$

(the isotropic level), at least from 0.3 to 10 AU [*Bavassano et al.*, 1982; *Klein et al.*, 1991, 1993; *Horbury et al.*, 1995; *Bruno et al.*, 1999; *Leamon et al.*, 1998; *Smith et al.*, 2006; *Hamilton et al.*, 2008; *MacBride et al.*, 2010]. Similar findings have been obtained for the plasma fluid velocity field $\boldsymbol{v}$, often with $A^v = \langle v_\perp^2\rangle/\langle v_z^2\rangle$ somewhat smaller than A^b. However, for this case a smaller number of measurements have been reported [e.g., *Klein et al.*, 1991]. (See *Oughton et al.* [2015, Table 2] for a summary of observational results.)

It is tempting to try to explain the appearance of variance anisotropy in the solar wind in terms of MHD turbulence theory, given that numerous other observed properties involving cascade, cross helicity, Alfvén ratio, and other quantities have been understood in this way [e.g., *Matthaeus and Goldstein*, 1982; *Sorriso-Valvo et al.*, 2007; *MacBride et al.*, 2008; *Marino et al.*, 2008, 2011; *Stawarz et al.*, 2009, 2010; *Osman et al.*, 2011a, 2011b; *Wan et al.*, 2012; *Bruno and Carbone*, 2013]. Variance anisotropy is a somewhat atypical property in that it is not readily found in simulations of *in*compressible turbulence, but rather, one must evidently appeal to compressible MHD turbulence effects to understand it. One finds, for example, that incompressible MHD with initial data having both isotropic variances and isotropic spectral distribution of energy does *not* lead to characteristic variance anisotropy, whereas compressible MHD does produce this effect [*Matthaeus et al.*, 1996].

An intriguing and subtle result in this regard emerges in the examination of the requirements for a compressible MHD medium to approach the condition of incompressibility at plasma beta (β) low or order 1 [*Zank and Matthaeus*, 1992, 1993]. In particular, one of these requirements is that the parallel variance must be suppressed by at least one power of the small expansion parameters in order that the incompressible limit be approached smoothly. While there is no guarantee that nature seeks this "nearly incompressible limit," the result is suggestive of the interplanetary observations. A related fact is that the parallel variance must be suppressed in order to derive the so-called reduced MHD (RMHD) equations [*Kadomtsev and Pogutse*, 1974; *Strauss*, 1976; *Zank and Matthaeus*, 1992], which are also incompressible and appropriate for low β plasmas. The interesting situation emerges that reduction of the parallel variance is evidently a requirement for approaching a dynamics that is well described by incompressible equations, and yet it also transpires that freely decaying compressible dynamics tends to evolve, at least partially, toward such a state. A corollary of these derivations is that when all fast timescales and all long (parallel) wavelength fluctuations are completely

removed from the 3-D MHD equations [*Zank and Matthaeus*, 1992], one may recover incompressibility only if the system completely two dimensionalizes (i.e., the parallel coordinate, z, becomes ignorable). In that case (and perhaps only in that case) the parallel fluctuations (b_z and v_z) evolve passively: being influenced by the 2-D transverse motions, but not having a reciprocal influence on those 2-D transverse motions.

The suggestion was made [*Matthaeus et al.*, 1996] that the parallel variance decays more rapidly in low Mach number compressible MHD due to separation of timescales between the compressible couplings versus the incompressible couplings. Such a mismatch makes it difficult to resupply energy to the inertial range of the compressive branch of the cascade. This finding implies that there are relatively weak couplings between parallel variance fluctuations and perpendicular variance fluctuations in compressible MHD at low turbulent Mach numbers and moderate to low β. This situation is analogous to the reduced coupling between compressive and incompressive motions in compressible hydrodynamics at low Mach number [*Ghosh and Matthaeus*, 1992]. However, we should note that a reduction of the rate of resupply of the compressive cascade does not imply that the cascades evolve completely independently. We revisit this point in section 5.

Variance anisotropy has also been studied from the perspective of wave modes. *Barnes* [1979] and *Barnes and Hollweg* [1974] studied the collisionless damping of the classical MHD wave modes when they are subjected to linear damping obtained from the Vlasov equation. The finding of relevance to the solar wind is that the slow modes are always heavily damped for interplanetary values of β, while fast modes are typically also damped relatively quickly. Various authors have argued [*Howes et al.*, 2012; *Klein et al.*, 2012] that slow modes in the solar wind survive only in the limit that they become degenerate with nonpropagating pressure balanced structures, which of course are not strictly to be considered waves. Indeed, such pressure balanced structures are already well known in turbulence as an essential element of the nearly incompressible limit alluded to above [*Zank and Matthaeus*, 1993]. Kinetic damping, in fact, may provide a ready explanation for the relative absence of propagating compressible modes in the solar wind, but of course, this explanation ignores turbulence completely. The simplified wave analysis also explains the origin of the term "magnetic compressibility" for the quantities such as $\langle b_z^2\rangle/\langle b_\perp^2 + b_z^2\rangle$, given that the only incompressible mode present in compressible MHD—the Alfvén mode—has zero parallel variance.

Variance anisotropy also enters in subtle ways in turbulence theories that are built up from wave theory. These are characterized by the enforcement of some wave properties, especially the dispersion relation, well into the highly nonlinear regime. In the context of *weak turbulence* and so-called *critical balanced* turbulence [*Sridhar and Goldreich*, 1994; *Goldreich and Sridhar*, 1995], one deals from the onset with the Alfvén mode and therefore exclusively with transverse variances. This approximation is initially a simple assumption but is justified later by an argument based on the fast, slow, and Alfvén linear dispersion relations [see *Goldreich and Sridhar*, 1995, section 5.3]. Their conclusion—that shear Alfvén modes produce an independent cascade—was subsequently examined in terms of a simplified mode identification scheme [*Cho and Lazarian*, 2002, 2003], who supported the same assumption of independence of the cascades of the different MHD mode types, for supersonic flows. This interpretation relies, of course, on the fluctuations remaining adequately described as wave-like, so that the mode identification is meaningful.

While there is a general concurrence that parallel variance in compressible MHD is associated with faster timescales and the presence of compressive effects, a number of questions and points of possible confusion persist. For example, it is unclear if the notion of independence of the parallel variance remains realizable in well-developed turbulence. Moreover, while an incompressible cascade is often viewed as consisting of modes that are, in some sense, Alfvén waves (or wave-like), it is important to recall that compressibility is apparently required for a dominant transverse variance to emerge dynamically [*Matthaeus et al.*, 1996] and that the approach to incompressibility requires bounding of the parallel variance [*Zank and Matthaeus*, 1992].

The main focus in the present study will be to further explore the connections relating variance anisotropy to properties of the well-developed turbulence cascade in MHD. We will show how, in decaying turbulence across a wide range of initial parameters, parallel variance comes into a kind of statistical quasi-equilibrium with transverse turbulence. The emergence of variance anisotropy favoring transverse polarizations as seen in the solar wind [*Belcher and Davis Jr.*, 1971] is typically also attended by other related turbulence properties including systematic connections to spectral anisotropy and Alfvén ratio (residual energy), and variations with plasma β, and we will briefly examine these connections.

Before delving into a description of the methods and results, we remark that there are other effects, notably those associated with inhomogeneities of turbulence, that can influence anisotropies, both of the variance and spectral types. In particular, it is well known that transport effects associated with turbulence in an expanding medium [*Zhou and Matthaeus*, 1989; *Velli et al.*, 1989; *Tu and Marsch*, 1995; *Verdini and Grappin*, 2015] influence variance anisotropy. At least some of the basic physics of these expansion effects can be seen even in the WKB theory of Alfvén waves in an expanding wind [*Völk and Aplers*, 1973]. Recently, the effects of expansion on the cascade have been explored using expanding box models [*Grappin and Velli*, 1996; *Dong et al.*, 2014; *Verdini et al.*, 2015; *Verdini and Grappin*, 2015]. Here we take a narrower tack, focusing on the effects associated with homogeneous turbulence [see *Oughton et al.*, 2015], which, although simpler, remain incompletely understood.

3. Simulations

The study is based on numerical experiments that employ a compressible, three-dimensional (3-D) spectral method code with a coordinate space resolution of 512^3 in a periodic cube of dimensionless side length 2π and a $\gamma = 5/3$ polytropic equation of state [e.g., *Ghosh et al.*, 1993]. In a standard notation, the dimensionless equations are

$$\frac{\partial \rho}{\partial t} = -\nabla \cdot (\rho \boldsymbol{v}), \tag{3}$$

$$\frac{\partial \boldsymbol{v}}{\partial t} = \boldsymbol{v} \times \boldsymbol{\omega} + \frac{\boldsymbol{j} \times \boldsymbol{B}}{\rho} - \nabla \left[C_1 \rho^{\gamma - 1} + \frac{v^2}{2} \right] + \frac{1}{\rho} \left[\nu_1 \nabla^2 \boldsymbol{v} + \nu_2 \nabla (\nabla \cdot \boldsymbol{v}) \right] \tag{4}$$

$$\frac{\partial \boldsymbol{a}}{\partial t} = \boldsymbol{v} \times \boldsymbol{B} + \eta \nabla^2 \boldsymbol{a} - \nabla \Phi, \tag{5}$$

where $\boldsymbol{\omega} = \nabla \times \boldsymbol{v}$, $\boldsymbol{B} = \boldsymbol{B}_0 + \boldsymbol{b}$, $\boldsymbol{b} = \nabla \times \boldsymbol{a}$, and $1/C_1 = (\gamma - 1) M_s^2$, with M_s a dimensionless parameter determining the initial sonic Mach number.

The main goal is to better understand how the parallel variance ingredient of turbulence either emerges or evolves when parameters such as mean magnetic field strength B_0, turbulent Mach number M_s, and plasma beta β are varied. The range of β explored, 0.25–16 for most runsets, is chosen for its relevance to the solar wind. (The solar wind is probably not a $\gamma = 5/3$ polytropic fluid; however, we expect that our results are relatively insensitive to the value of γ.)

As is well known, spectral method simulations with genuine discontinuities are associated with Gibbs phenomenon overshoot [e.g., *Passot and Pouquet*, 1987; *Ghosh and Matthaeus*, 1992; *Canuto et al.*, 1988]. However, since our simulations have nonzero dissipation coefficients, shocks and other sharp structures (e.g., current sheets) are spread over at least several grid points. We have chosen the viscosity and resistivity values conservatively to ensure that this is the case. Specifically, for all runs discussed herein, $\nu_1 = \nu_2 = \eta = 0.002$ and for the initial fluctuations employed this yields initial large-scale Reynolds numbers of ≈ 200. Many one-dimensional density profiles from various runs have been examined with no indication of any resolution issues.

3.1. Initial Conditions

We have carried out a large number of runs with several different classes of initial conditions (ICs). In all cases the initial mass density is $\rho = \rho_0 = 1$ and the initial excited bandwidth range is $3 \leq |\boldsymbol{k}| \leq 9$ (in box size units). Excitation is spectrally isotropic, except for the quasi-2-D classes—see case 4 below. The runsets also differ in the choice of variance anisotropy, with the initial $\tilde{\boldsymbol{v}}(\boldsymbol{k})$ and $\tilde{\boldsymbol{b}}(\boldsymbol{k})$ polarizations as follows:

1. toroidal (aka Alfvénic), meaning in the $\boldsymbol{k} \times \boldsymbol{B}_0$ direction;
2. isotropic, approximately equal energy in the toroidal and poloidal components (but no longitudinal $\boldsymbol{v}$ excitation);
3. either of the above but with either half or all of the velocity energy in the longitudinal (compressive) modes (respectively denoted "Hlong" and "Along" in Table 1); or
4. a mixture of quasi-2-D + quasi-isotropic initial conditions. Here 80% of the energy is in the $k_z = 0$ modes and toroidally polarized, with the other 20% in the $|k_z| > 0$ modes, with isotropic polarizations. A second IC of this form uses $|k_z| \leq 1$ as the quasi-2-D modes (denoted "q2d-kz0" and "q2d-kz1" in Table 1).

Cases 2 and 3 are similar to lower resolution simulations reported in *Matthaeus et al.* [1996]. Table 1 lists the major parameters for the runs, organized by runset, along with typical evolved values for some anisotropy-related quantities to be discussed.

Table 1. Values of Selected Quantities at $t = 2t_{\max D}$ (Except the Final Two Columns Which Are $t = 0$ Values)[a]

IC Type	$t_{\max D}$	$t^b_{1/2}$	$t^v_{1/2}$	A_b	A_v	$b^2_{\rm tor}/b^2$	$v^2_{\rm tor}/v^2$	$u^2_{\rm long}/v^2$	2Dfrac	v^2/b^2	$\delta\rho/\rho_0$	$\delta b/B_0$	B_0	M_s	β
Toroidal	0.75	0.7	0.65	6.5	5.7	0.8	0.77	0.0077	0.064	0.86	0.013	0.76	1	0.15	44
Toroidal	0.75	0.7	0.65	6.7	5.6	0.81	0.76	0.024	0.066	0.87	0.036	0.76	1	0.25	16
Toroidal	0.8	0.7	0.75	7.7	5.1	0.83	0.73	0.064	0.072	0.85	0.11	0.73	1	0.5	4
Toroidal	0.8	0.7	0.7	8.5	5.9	0.84	0.76	0.081	0.079	1	0.12	0.5	1.4	0.5	2
Toroidal	0.85	0.55	0.65	10	6.5	0.86	0.76	0.1	0.092	1	0.12	0.36	2	0.5	1
Toroidal	0.95	0.4	0.5	11	9	0.88	0.79	0.11	0.097	1	0.11	0.24	3	0.5	0.44
Toroidal	1.1	0.35	0.7	13	10	0.9	0.81	0.1	0.11	0.95	0.11	0.18	4	0.5	0.25
Isotropic	0.75	–	–	1.8	1.6	0.56	0.51	0.015	0.057	0.89	0.016	0.69	1	0.15	44
Isotropic	0.75	–	–	1.9	1.6	0.56	0.49	0.041	0.059	0.92	0.042	0.68	1	0.25	16
Isotropic	0.75	0.05	–	2.2	1.6	0.6	0.49	0.077	0.061	0.99	0.13	0.66	1	0.5	4
Isotropic	0.8	0.05	–	2.5	1.9	0.63	0.52	0.093	0.075	1.2	0.14	0.45	1.4	0.5	2
Isotropic	0.8	0.05	–	3.2	1.8	0.7	0.51	0.12	0.081	1.2	0.16	0.32	2	0.5	1
Isotropic	0.8	0.05	–	4.7	2	0.77	0.53	0.15	0.079	1.2	0.17	0.22	3	0.5	0.44
Isotropic	0.75	0.05	–	5.1	2.4	0.77	0.55	0.13	0.079	1.3	0.17	0.17	4	0.5	0.25
tor-Hlong	0.85	0.75	–	7	5.4	0.81	0.68	0.17	0.077	1.2	0.074	0.64	1	0.25	16
tor-Hlong	0.75	0.1	–	8.9	5.5	0.84	0.7	0.14	0.078	0.97	0.14	0.5	1.4	0.5	2
tor-Hlong	0.7	0.1	0.05	8.6	6.6	0.83	0.73	0.14	0.083	1.1	0.14	0.35	2	0.5	1
tor-Hlong	0.85	0.05	0.05	9.3	6.8	0.85	0.73	0.15	0.095	1	0.12	0.24	3	0.5	0.44
tor-Hlong	0.75	0.05	0.05	8.7	7.6	0.85	0.74	0.15	0.094	1.1	0.13	0.19	4	0.5	0.25
tor-Along	0.6	0.35	0.1	11	4.7	0.86	0.56	0.35	0.082	1.3	0.09	0.58	1	0.25	16
tor-Along	0.4	0.1	0.1	8.8	5	0.83	0.57	0.34	0.071	1.3	0.19	0.65	1	0.5	4
tor-Along	0.35	0.05	0.1	5.4	7.6	0.73	0.61	0.27	0.069	1.4	0.17	0.34	2	0.5	1
tor-Along	0.35	0.05	0.1	4.8	5.2	0.73	0.61	0.27	0.065	1.1	0.18	0.25	3	0.5	0.44
tor-Along	0.35	0.05	0.1	4.1	5.3	0.8	0.34	0.28	0.067	1.3	0.17	0.18	4	0.5	0.25
q2d-kz0	0.65	0.65	0.5	8.7	4.8	0.86	0.73	0.042	0.42	0.58	0.039	0.85	1	0.25	16
q2d-kz0	0.7	0.1	0.5	8.9	4.4	0.87	0.7	0.08	0.43	0.61	0.11	0.82	1	0.5	4
q2d-kz0	0.7	–	0.45	11	5	0.89	0.74	0.075	0.52	0.63	0.12	0.58	1.4	0.5	2
q2d-kz0	0.7	–	0.4	13	5.6	0.91	0.77	0.076	0.59	0.61	0.12	0.41	2	0.5	1
q2d-kz0	0.6	–	0.3	15	7.8	0.92	0.8	0.076	0.66	0.62	0.11	0.29	3	0.5	0.44
q2d-kz0	0.6	0.05	0.1	20	9.5	0.94	0.81	0.081	0.7	0.6	0.1	0.22	4	0.5	0.25
q2d-kz1	0.8	0.85	0.6	5.9	4.1	0.81	0.71	0.034	0.15	0.64	0.037	0.77	1	0.25	16
q2d-kz1	0.85	0.8	0.6	6.6	3.9	0.82	0.69	0.065	0.15	0.68	0.11	0.73	1	0.5	4
q2d-kz1	0.8	0.7	0.45	7.4	4.5	0.85	0.73	0.064	0.18	0.81	0.11	0.51	1.4	0.5	2
q2d-kz1	0.8	0.1	0.4	10	5.3	0.89	0.76	0.073	0.2	0.83	0.12	0.35	2	0.5	1
q2d-kz1	0.8	–	0.45	13	7.1	0.91	0.8	0.072	0.23	0.9	0.11	0.24	3	0.5	0.44
q2d-kz1	0.75	–	0.4	15	9.6	0.91	0.83	0.07	0.22	0.91	0.11	0.19	4	0.5	0.25

[a] $t^{b,v}_{1/2}$ are the times taken for the corresponding quantity $A^b = \langle b^2_\perp\rangle/\langle b^2_z\rangle$ or A^v to approach within 50% (above or below) of its value at $2t_{\max D}$. A dashed line in the $t_{1/2}$ columns indicates that $A^{b,v}$ is always within this range. 2Dfrac is the fraction of the fluctuation energy in the (strictly) 2-D modes and $\delta b = \sqrt{\langle b^2\rangle}$. For readability of the column headings, the $\langle\rangle$ symbols which should appear around b^2, etc., have been suppressed.

We emphasize that our initial conditions are *not* a sum of linear wave eigenmodes. At each excited wave vector, the $\tilde{b}_t$, $\tilde{b}_p$, $\tilde{v}_t$, and $\tilde{v}_p$ are set using independent Gaussian random variables (subject to a spectral shape function) [see *Matthaeus et al.*, 1996, equation (6)], so that wave eigenmode relationships are not imposed. This approach stands in contrast to that of *Cho and Lazarian* [2002, 2003] who initialized simulations using superpositions of wave modes.

3.2. Diagnostics

All runs have an initial Alfvén ratio $r_A = E^v/E^b$=1, where $E^v = \langle\rho\boldsymbol{v}\cdot\boldsymbol{v}\rangle/2$ and $E^b = \langle\boldsymbol{b}\cdot\boldsymbol{b}\rangle/2$ are the fluctuation kinetic and magnetic energies and $\langle\cdots\rangle$ is the average over the spatial domain. Other useful quantities

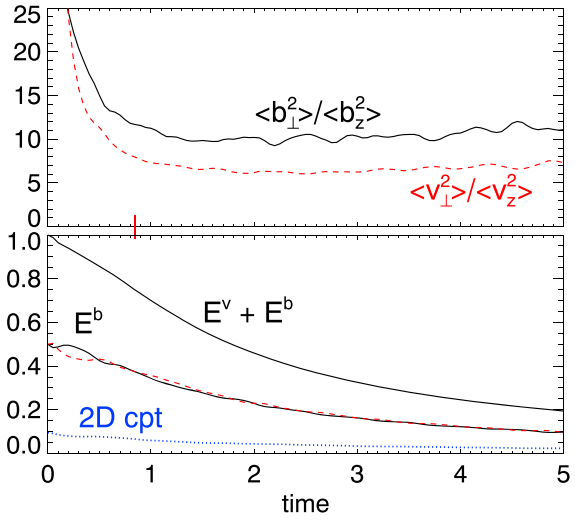

Figure 1. Evolution of variance anisotropies and fluctuation energies from a compressible 3-D MHD run with toroidal ICs for $\boldsymbol{v}$ and $\boldsymbol{b}$. The run has $B_0 = 2$, $M_s = 0.5$, and $\beta = 1$. The (red) tick on the time axis, near $t = 1$, is the time of maximum energy dissipation, $t_{\max D}$. Note the saturation of the variance anisotropy after about a nonlinear time, even though the energy shows significant ongoing decay.

we refer to include the mean-square longitudinal velocity $\langle u^2_{\rm long}\rangle = \sum_{\boldsymbol{k}} |\tilde{\boldsymbol{u}}_L(\boldsymbol{k})|^2$, the toroidal energies $\langle b^2_{\rm tor}\rangle = \sum_{\boldsymbol{k}} |\tilde{b}_t(\boldsymbol{k})|^2$ and $\langle v^2_{\rm tor}\rangle = \sum_{\boldsymbol{k}} |\tilde{v}_t(\boldsymbol{k})|^2$, with analogous expressions for the poloidal energies, and the RMS density fluctuation $\delta\rho = \langle(\rho - \rho_0)^2\rangle^{1/2}$. Also revealing are the Alfvén ratios for the toroidal component and the 2-D component,

$$r_A^{\rm tor} = \frac{\rho_0\langle v^2_{\rm tor}\rangle}{\langle b^2_{\rm tor}\rangle}, \quad r_A^{\rm 2D} = \frac{\rho_0 \sum_{\boldsymbol{k}} |\tilde{\boldsymbol{v}}_\perp(k_z = 0)|^2}{\sum_{\boldsymbol{k}} |\tilde{\boldsymbol{b}}_\perp(k_z = 0)|^2}. \tag{6}$$

For this study, we define 2-D to mean the transverse (x and y) components of the $k_z = 0$ portions of $\boldsymbol{v}$ and $\boldsymbol{b}$. These are sometimes called the *strictly* 2-D modes, since they exclude the contributions from the out-of-plane components $v_z(k_z = 0)$ and $b_z(k_z = 0)$. When the v_z and b_z components are included, the fluctuations are termed 2.5-D. Note that the 2-D and toroidal components are not mutually exclusive since when $k_z = 0$, the toroidal component is also a 2-D component.

Conventionally, Alfvén ratios are defined using the kinetic energy rather than the mean-square velocities (and average density, $\rho_0 = 1$) employed in equation (6). We choose these forms for several reasons. First, the density fluctuations are small and thus are not expected to have a large impact on the Alfvén ratios. Second, since toroidal fluctuations are solenoidal, their velocity is incompressible, meaning density fluctuations are not directly relevant to their dynamics. Third, there is the practical point that, as defined, $r_A^{\rm tor}$ and $r_A^{\rm 2D}$ are computationally simple to calculate. We also find that for all the runs considered herein there is no significant difference between the true (total) Alfvén ratio $r_A = E^v/E^b$ and $\rho_0\langle v^2\rangle/\langle b^2\rangle$.

4. Results

4.1. Growth and Saturation of Parallel Variance

To set the context, we show in Figure 1 some sample behavior for a "toroidal" run, with $B_0 = 2$, $M_s = 0.5$, and $\beta = 1$. Additional characteristics for the run are given on line five of Table 1. The other toroidal IC runs listed in the table evolve in roughly the same way as this sample run.

The run begins with strictly toroidal fluctuations and thus no parallel variances. From Figure 1 (top) we observe that the parallel variance of both the magnetic fluctuations and the velocity fluctuations increases until about 10–15% of the fluctuation energy is in the parallel components. This occurs in one or two $t_{\max D}$, where this is the time of maximum dissipation for the run, usually a reasonable measure of the actual nonlinear time; a red tick on the time axis indicates $t_{\max D}$. It is revealing that after this characteristic time, the variance anisotropies are rather stable and remain so throughout the time period displayed. This is in contrast to the fluctuation turbulence energies for the same run, which show ongoing decay (Figure 1, bottom). The contributions from the velocity, magnetic, and (strictly) 2-D ingredients are all indicated.

A closer look at the generation of parallel variance for the same run is given in Figure 2. In Figure 2 (top row) we see that the two transverse components are nearly equal, while the parallel variance saturates at levels just less than one tenth the total for the magnetic field and a little greater than one tenth for the velocity field. The presence of a parallel variance in solar wind turbulence is often referred to as a "compressive component," as it is reminiscent of magnetosonic waves. Indeed, here we see that the relative density fluctuation, initially zero, increases to about 15% near $t = t_{\max D}/2$, somewhat earlier than the time of saturation of the variance anisotropy, and gently decreases thereafter.

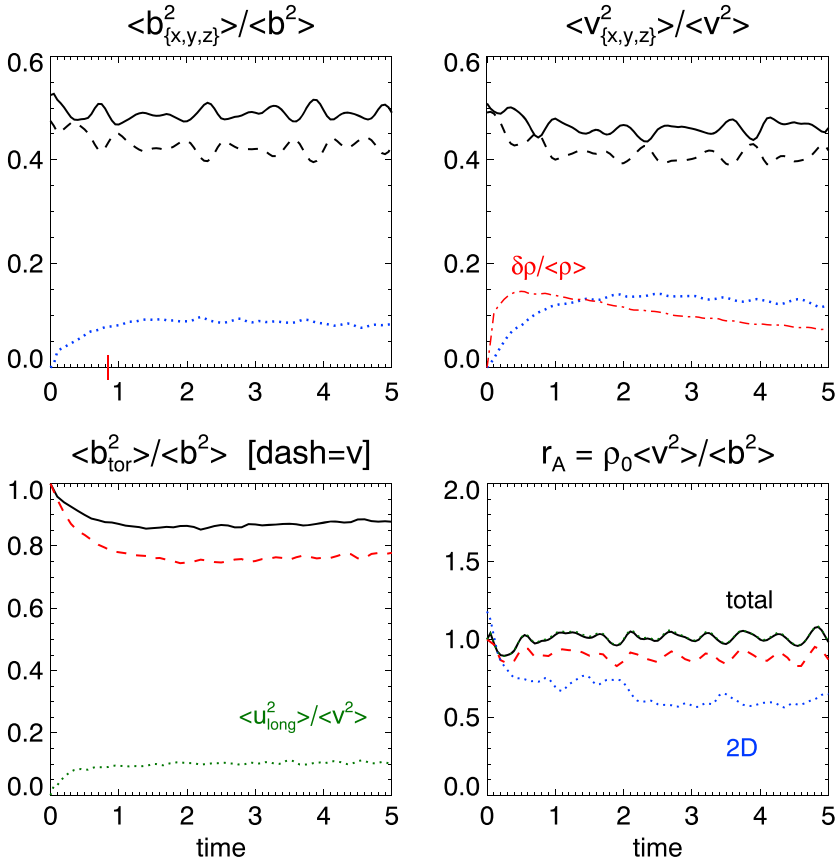

Figure 2. Time histories for variance-related quantities from the same run used in Figure 1. (top tow) The x, y, z components are depicted using solid, dashed, and dotted line styles, respectively. (bottom right) The dashed (red) curve is r_A^{tor}.

From Figure 2 (bottom left) one sees that the toroidal (or Alfvénic) fraction, for both the magnetic field and the velocity field, decreases a little from its initial value of 100% but remains large throughout the run. Accordingly, the energy in the longitudinal part of the velocity, $\langle u^2_{long} \rangle$, remains small, at the ~10% level in this case. Also noteworthy is that the longitudinal fluctuations (and the parallel fluctuations) were initially absent: they have been generated from zero. This indicates that parallel/compressive fluctuations are not just passively advected by the Alfvénic fluctuations, as has sometimes been argued [e.g., *Goldreich and Sridhar*, 1995; *Lithwick and Goldreich*, 2001].

Figure 2 (bottom right) displays Alfvén ratios associated with three different subsets of the fluctuations and serves to further describe the nature of the turbulence. The total Alfvén ratio, $r_A = \rho_0 \langle v^2 \rangle / \langle b^2 \rangle$, hovers near unity for most of the run. However, the toroidal fluctuations have an Alfvén ratio, r_A^{tor}, that is persistently slightly under unity. The reason for this, in the present run, is largely due to the 2-D component (a contributor to the toroidal component), which displays an r_A^{2D} that drops from an initial value of 1 to around $r_A^{2D} \sim 0.7$ and remains at that level or slightly lower. All the runs reported on here display this feature of low r_A^{2D}. This may be due to the presence of strong current sheets and component reconnection in the 2-D component, as it has been suggested [*Matthaeus and Lamkin*, 1986] that low Alfvén ratio is associated with these features. We consider this further in section 4.3.

4.2. Scalings With β

Having shown some typical evolution and saturation behavior for quantities of interest, we now present summary plots indicating how these saturation levels vary with the initial plasma beta, $\beta = 1/(B_0 M_s)^2$. For these dissipative initial value computations, the time-varying β generally increases, since energy dissipation causes

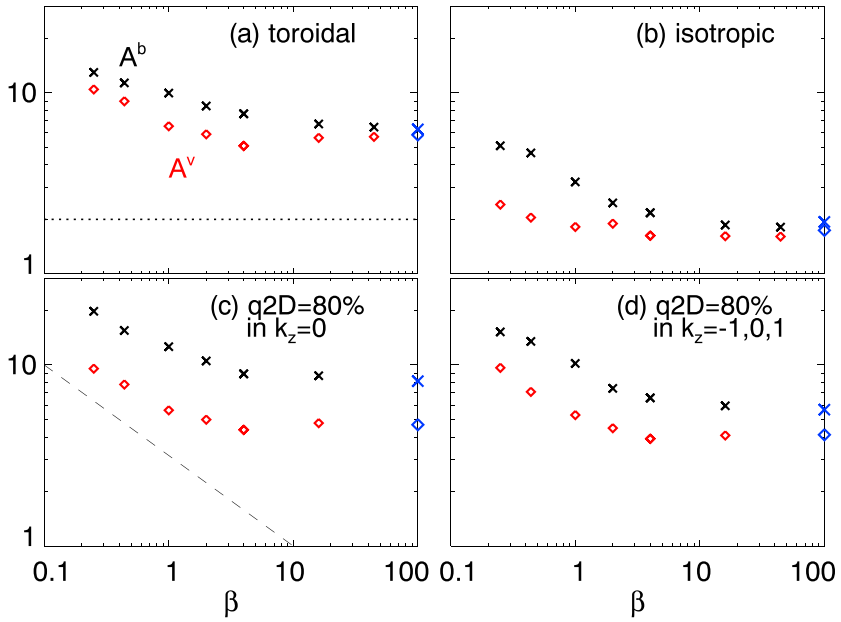

Figure 3. Anisotropy ratios for the magnetic (A^b—crosses) and velocity (A^v—diamonds) fluctuations as a function of β. Each panel is for a different type of ICs. Values are computed at $t = 2t_{\max D}$. The (blue) symbols on the $\beta = 100$ axis are from incompressible $B_0 = 1$ simulations with identical ICs to the rest of the runs employed in that panel. The dotted line in Figure 3a is the value associated with variance isotropy. The dashed line in Figure 3c is a reference $\beta^{-1/2}$ scaling.

the Mach number to decrease. The values shown in these summary plots are computed at $t = 2\,t_{\max D}$ for each run. In each figure, results from four particular runsets are displayed, with their IC classes being toroidal, isotropic, and the two sorts of quasi-2-D + quasi-isotropic.

Figure 3 shows the variance anisotropy ratios, $A^b = \langle b_\perp^2\rangle/\langle b_z^2\rangle$ and A^v. For the toroidal ICs case, Figure 3a, one sees a roughly β-independent saturation level when $\beta \gtrsim 10$, and an increase of the quantities as β decreases. The dotted line in this panel is the value for the case of isotropic variances ($A^b = 2$), and all values are well above it. This basic trend is the same in each of the other panels, although for the isotropic ICs the initial variance isotropy persists at higher β for both fields and for most lower values of β for the velocity fluctuations. At a given β, Figures 3a, 3c, and 3d also show quantitatively similar values for A^v, indicating only a weak dependence on these IC classes; the A^b values show greater quantitative variation across the runsets. In particular, Figure 3c with quasi-2-D defined as just the $k_z = 0$ modes shows the largest values for A^b.

In all cases shown we have $A^b > A^v$, which is in accord with solar wind observations at MHD scales [*Klein et al.*, 1991; *Bruno et al.*, 1999]. Furthermore, there is even approximate quantitative agreement between the observations and those simulations with toroidal ICs or quasi-2-D ICs. Naturally, runs with substantial amounts of initial $\langle u_{\rm long}^2\rangle$ have a greater degree of compressive activity and sometimes show more complicated behavior than the cases displayed in Figure 3 (see Table 1).

The symbols on the $\beta = 100$ axis are results from $B_0 = 1$ incompressible simulations with the same initial conditions as the rest of the runs in the panel. These values suggest that as β gets large, A^b and A^v approach their incompressible analogs.

Next we consider the scaling of several energy fractions with β (Figure 4). It is apparent that the toroidal energy is always dominant over the poloidal (and longitudinal) energies, with $\langle b_{\rm tor}^2\rangle/\langle b^2\rangle \approx 60$–$90\%$ and $\langle v_{\rm tor}^2\rangle/\langle v^2\rangle \approx 50$–$80\%$. This holds for all IC classes investigated, not just those shown in the figure, even when it is not true of the initial state. (There is one exception: a $\beta = 0.25$ run, with toroidal $\boldsymbol{b}$, but purely longitudinal $\boldsymbol{v}$ ICs.) See Table 1. Generally, there is a weak increase of the toroidal fractions with decreasing β, with the isotropic ICs showing the strongest effect. For the poloidal energy fractions (not shown), the behavior is similar although the levels are of course small. Again, the magnetic version is usually somewhat larger than the velocity one.

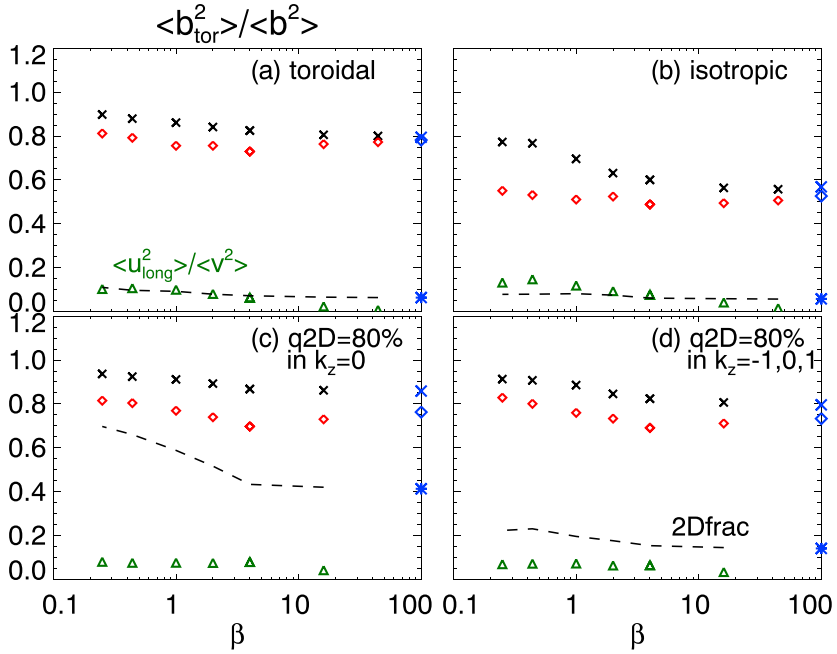

Figure 4. As in Figure 3, except showing fraction of magnetic energy in the toroidal (aka Alfvénic) component (crosses) and similarly for the mean-square velocity (red diamonds). Also shown are mean-square longitudinal velocity fractions (green triangles) and the fraction of energy in the strict 2-D modes (dashed line). Most IC classes show relatively weak β dependence. As β increases, the quantities approach the associated incompressible values shown (in blue) on the $\beta = 100$ axes.

One also sees that within each studied runset, the energy fraction for the longitudinal velocity, $\langle u^2_{\rm long}\rangle/\langle v^2\rangle$, is almost independent of β, when $\beta \lesssim 10$ (triangles). The same is also true for the relative density fluctuations (not shown; see Table 1). This may be connected with the Mach number, since the $\beta \lesssim 10$ runs all have the same initial $M_s = 0.5$, while the runs with larger β have lower values of M_s. Recall that nearly incompressible (NI) theory predicts $\delta\rho = O(M_s^2)$ [*Zank and Matthaeus*, 1993]. In any case, whether the initial velocity has no longitudinal component or is 100% longitudinal, the systems evolve to states where $\langle u^2_{\rm long}\rangle$ is a small or modest component, with the toroidal component (of $\boldsymbol{v}$ and $\boldsymbol{b}$) being energetically predominant. In this sense, the dynamical importance of the toroidal component is independent of compressive velocity fluctuations that may or may not be present initially.

Results from low-β *super*sonic simulations [*Cho and Lazarian*, 2002] indicate a similar weak dependence on β for $(\delta V)^2_{\rm fast}/(\delta V)^2_{\rm Alf}$, where these are the energies associated with fluctuations polarized in the same sense as fast modes and Alfvén waves. In our notation this is approximately $\langle u^2_{\rm long}\rangle/\langle v^2\rangle$, because when β is small, one has $(\delta V)^2_{\rm fast} \approx \langle u^2_{\rm long}\rangle$, assuming the usual spectral anisotropy, $\boldsymbol{k} \approx \boldsymbol{k}_\perp$. The denominator has been replaced with $\langle v^2\rangle \approx \langle v^2_{\rm tor}\rangle$ since the toroidal energy dominates in both their work and ours. On the other hand, *Cho and Lazarian* [2002] find that $(\delta V)^2_{\rm fast}/(\delta V)^2_{\rm Alf} \propto \delta b/B_0$, whereas we do not observe an equivalent relationship (see Table 1).

One further feature is indicated in Figure 4: the energy fraction for the 2-D component (dashed lines). For all cases shown, decreasing β leads to a slightly bigger 2-D fraction, although still weaker than the initial level for the particular run. This latter point suggests that it may be difficult to generate a substantial 2-D component from states with low initial levels, at least in the absence of driving. On the other hand, when the 2-D fraction is initially high—as in the "80%" cases of Figure 4c—the $t = 2\,t_{\rm max\,D}$ levels are still substantial, especially for $\beta \lesssim 1$. As in the previous figure, $B_0 = 1$ incompressible results are marked on the $\beta = 100$ axes and reveal that these are approached at large β.

Observational solar wind results at distances of 0.3–1 AU typically indicate that when the fluctuations are modeled as an admixture of 2-D modes and parallel-propagating slab waves, the 2-D component is dominant, often at the 80–95% level [*Bieber et al.*, 1996] (see *Oughton et al.* [2015] for a review of similar studies).

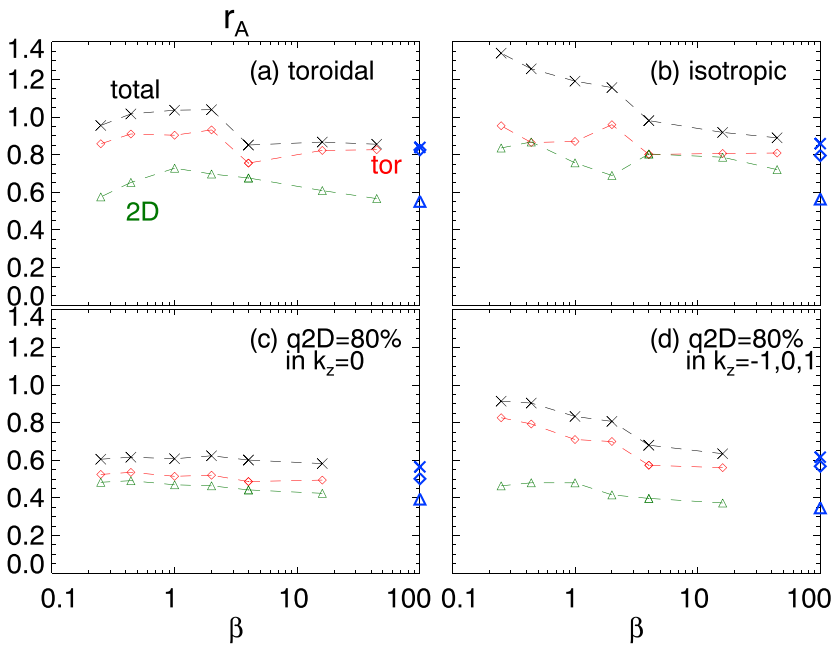

Figure 5. As in Figure 3 except showing the Alfvén ratios r_A for all the fluctuations (crosses), the toroidal component (red diamonds), and the 2-D component (green triangles). Only the dominantly 2-D IC class shows total r_A values quantitatively similar to those observed in the solar wind. At high β there is again a strong correspondence with the values from the incompressible runs (blue symbols on $\beta = 100$ axis).

Since solar wind fluctuations undergo transport outward from the Sun, the results presented here suggest that the observed high levels of a 2-D component may also need to be present at small heliocentric distances. Driving (e.g., by stream shear) is another way that a high 2-D fraction could be generated.

4.3. Relation to Alfvén Ratio (Residual Energy)

Figure 5 illustrates the behavior of the Alfvén ratios at $t = 2\,t_{\max D}$ for several types of initial data we have investigated. In all four panels, one can see the ordering $r_A^{2D} \le r_A^{tor} \le r_A$, indicating that it is the 2-D modes that are farthest from kinetic-magnetic energy equipartition. In addition, the β dependence of r_A^{2D} is rather weak, as is its variation with IC type. The situations for r_A and r_A^{tor} are more involved, with r_A^{tor} usually less than unity, and the toroidal ICs and isotropic ICs sometimes having $r_A > 1$ at $\beta \lesssim 2$. Examination of the k_z dependence of r_A^{tor} (not shown) indicates that it is the 2-D component that is responsible for r_A^{tor} being less than unity, with $r_A^{tor}(k_z \neq 0) \approx 1$. As before, the symbols on the $\beta = 100$ axes denote $B_0 = 1$ incompressible results.

Similar results have been reported for simulations of incompressible homogeneous MHD turbulence [e.g., *Oughton et al.*, 1994; *Bigot et al.*, 2008]. In particular, one finds $r_A \approx 1$ for runs with $\delta b/B_0 < 1$ and that $r_A^{2D} < 1$ for essentially all values of $\delta b/B_0$ investigated [*Bigot et al.*, 2008; *Bigot and Galtier*, 2011].

As Figure 5 clearly displays, r_A^{2D} is always significantly smaller than unity and often quantitatively similar to the level of $\approx 1/2$ commonly observed in the solar wind beyond ≈ 0.5 AU [*Matthaeus and Goldstein*, 1982; *Roberts et al.*, 1987a, 1987b; *Perri and Balogh*, 2010]. However, it is only for the $k_z = 0$ type quasi-2D ICs, Figure 5c, that we find a total Alfvén ratio of about this level. Furthermore, there is very little dependence on β (or $\delta b/B_0$; see Table 1) for this IC class.

Thus, our results indicate that of the cases investigated, only dominantly quasi-2-D fluctuations produce Alfvén ratios that are consistent with solar wind MHD-scale observations. Moreover, this class of ICs also leads to reasonable quantitative agreement with observed values for A^b and A^v.

Various explanations for why $r_A < 1$ have been advanced, including local in $\boldsymbol{k}$-space dynamo action [*Pouquet et al.*, 1976; *Grappin et al.*, 2016], small-scale reconnection, with current sheets more intense than the nearby vorticity coherent structures [*Matthaeus and Lamkin*, 1986], and a perturbation theory approach that indicates two counterpropagating Alfvén waves drive a $k_z = 0$ purely magnetic structure [*Howes and Nielson*, 2013; *Nielson et al.*, 2013]. For the case of solar wind fluctuations, *Yokoi* [2011] has shown that an approximately

distance-independent value of $r_A \approx 1/2$ emerges as a consequence of balance between the dominant terms in a (time steady) transport equation for the energy difference, $E^v - E^b$ (equivalent to r_A). On the empirical side, an observational study [*Roberts*, 2010] indicates that r_A changes with heliocentric radius mostly because (radial) spectral evolution of $E^v(k)$ is stronger than that for $E^b(k)$.

4.4. Relation to Spectral Anisotropy

In section 1 we remarked that variance anisotropy and spectral anisotropy are independent at a kinematic level. For example, one may easily construct synthetic spectra that admit one type of anisotropy but not the other. (Here synthetic means that the Fourier components have not been determined from the dynamical equations.) However, in the above description of *dynamical* results, we have found that such connections do exist. In particular, the 2-D part of the energy spectrum—consisting of those Fourier modes that have zero parallel wave number—appears to have special status regarding this connection. This highly anisotropic sample of the spectral wave vectors also shows the strongest variance anisotropy, favoring the perpendicular variances. The same modes also exhibit the lowest values of Alfvén ratio.

5. Discussion and Conclusions

In this paper we have studied variance anisotropy in compressible 3-D MHD simulations from a few different perspectives. The first and perhaps most significant result pertains to undriven MHD turbulence initiated with entirely transverse (toroidal) variances in magnetic and velocity fluctuations. In the MHD regime such a state is often called "Alfvénic," referring to the linear modes that admit this transverse property. We find that parallel variance, absent initially, is generated in timescales comparable to the large-scale eddy-turnover (or nonlinear) timescale. The level of parallel variance attained is typically near 10% of the perpendicular variance level (with a range of about 5% to 20%) for the parameters we have examined, and this level remains remarkably stable during the subsequent decay of the turbulence energy. For runs with varying initial turbulence amplitudes, $\delta b/B_0 \sim 0.25-1.0$, and varying values of plasma beta, $\beta \sim 0.25-16$, this description of the behavior of the variance anisotropy does not change greatly.

The above result is complementary to an earlier finding [*Matthaeus et al.*, 1996] regarding the evolution of the same model—compressible MHD with a moderately strong mean magnetic field—when initialized with an isotropic variance, $\langle b_\perp^2 \rangle = 2\langle b_z^2 \rangle$, and similarly for the velocity fluctuations. In that case it was found that the evolution is toward a reduced parallel variance for both $\boldsymbol{v}$ and $\boldsymbol{b}$ and that it occurs on essentially the nonlinear timescale. For $\langle b_z^2 \rangle$ there is also a short adjustment phase during which it drops sharply. This ceases at $t \approx 0.1$ (the same timescale over which the density fluctuations increase from zero) and is followed by a gradual recovery, on the nonlinear timescale, and then subsequent decay. Interestingly, the behavior for $t \gtrsim 0.1$ is suggestively similar to that seen in the cases with transverse initial conditions.

The point to note is that both processes—increase of parallel variance from an initial transverse state and the reduction of parallel variance from an initial isotropic state—occur on timescales of a few global nonlinear times, i.e., the turbulent cascade and energy decay timescale. In each case the realized values of parallel variance are small but by no means negligible, with the RMS parallel fluctuation amplitude about one third to one half of the RMS value of each of the perpendicular component amplitudes. Not only does this suggest that the generation and maintenance of the parallel variance is intrinsically a property of turbulence decay and cascade but it is also rather interesting that the range of relative values of the variances is quite comparable to the classic "5:4:1" partitioning identified by *Belcher and Davis Jr.* [1971] in the solar wind.

A second finding is that the magnetic variance anisotropy ratios, $A^b = \langle b_\perp^2 \rangle / \langle b_z^2 \rangle$, are larger when β is small and essentially monotonically decreasing with increasing β. This is completely consistent with a familiar idea in hydrodynamic turbulence that the mechanical pressure drives the variances toward isotropy, while advective terms drive energy cascade [*Batchelor*, 1970]. Decrease of variance anisotropy with increasing β is also observed in the solar wind [*Smith et al.*, 2006], seemingly with a somewhat steeper falloff there, $\sim \beta^{-0.7}$, although the solar wind data extended to considerably lower values of β compared to the simulation cases we have reported on. For the simulation values of A^v, the trends are the same as the A^b ones, but the monotonic decrease with increasing β is only approximate.

Another point of discussion related to the first topic above is the degree to which, in MHD, the parallel variance is an independent element of the turbulence, and the related (but not identical) issue of whether highly oblique Alfvén modes evolve separately from magnetosonic modes. We know that for incompressible 2.5-D

MHD the parallel variance is exactly independent [*Montgomery and Turner*, 1982]. Similarly, in the context of Reduced MHD [*Montgomery*, 1982; *Zank and Matthaeus*, 1992; *Schekochihin et al.*, 2009], which is a weakly three-dimensional model, with wave vectors slightly removed from 90° to the mean field, the parallel variance ingredient decouples completely at the order of the retained effects. In spite of these suggestive incompressible limiting cases, the compressible results summarized above do not support a conclusion that the parallel variance fluctuations evolve completely independently as suggested previously based on wave theory or wave-dominated weak turbulence theory [*Goldreich and Sridhar*, 1995, 1997; *Cho and Lazarian*, 2002, 2003].

Indeed, one observation in support of this nonindependence, made here and earlier [*Matthaeus et al.*, 1996], is that the fully isotropic compressible case evolves toward a stable value of variance anisotropy ratio. The fact that this ratio is stable and the fraction of parallel variance is not monotonically decreasing with time implies that parallel variance is being resupplied from the perpendicular variances, since otherwise the decay rates for the parallel and perpendicular components would be expected to differ. Also implied is that this energy transfer rate is comparable to some constant fraction of the cascade rate of the total fluctuation energy. Furthermore, a very similar argument applies to the case examined in the present paper, with initial transverse variance. Here the conclusion is evidently that the parallel variance is generated on a timescale comparable to the incompressible turnover time. The overall picture is consistent with the conclusion that parallel variance is coupled to the incompressible cascade at a suppressed (but nonvanishing) rate, but one that is nonetheless a nearly constant fraction of the incompressible cascade rate itself.

A stronger assumption, apparently incorrect for the simulations reported on here, made by several authors [*Goldreich and Sridhar*, 1997; *Lithwick and Goldreich*, 2001; *Cho and Lazarian*, 2002, 2003], that the non-Alfvénic modes are independent, may have seemed appealing based on linear wave theory. However, that approach necessarily ignores certain nonlinear effects that are not described in linear theory. Relevant examples are not difficult to identify. Quasi-two-dimensional pressure balanced parallel velocity shears are nonpropagating in linear theory but can contribute to a nonlinear cascade [see, e.g., *Ghosh et al.*, 1998a, 1998b], and the nonlinear incompressible pressure constraint is responsible for nonpropagating density fluctuations known as pseudosound [*Lighthill*, 1952; *Montgomery et al.*, 1987].

There are also other avenues to explore regarding variance anisotropy, preponderance of toroidal fluctuations, and Alfvén ratios. In particular, the extent to which the features and behavior we have presented here are associated with possible linear wave mode activity. This could be pursued by calculating various correlations. However, even when such correlations are found, there can be a multiplicity of explanations. For example, density-$|\boldsymbol{B}|$ anticorrelations might indicate either a propagating magnetosonic mode [e.g., *Klein et al.*, 2012] or a pseudosound nonpropagating response of the density—as described by nearly incompressible (NI) theory [*Zank and Matthaeus*, 1993]. Alternatively, depending on how things vary with Mach number, the anticorrelation could indicate a mixture of these, which might be consistent with NI theory, or not. To further complicate things, the sense of correlation might change with scale and with direction of variance or direction of gradient (wave vector). Wave theorists might also argue that when analyzing the correlation as a function of wave vector direction, the proper way to do it is relative to local field. We intend to investigate these issues in the future.

In summary, our current conclusion, stated above, is that the parallel variance fluctuations in MHD admit a finite strength (although partially suppressed) coupling to the nearly incompressible transverse variance fluctuations. This conclusion is based on a fully nonlinear assessment and is undistracted by special properties of linear waves. When the level of parallel variance is not consistent with the amount that is compatible with the cascade at a specified β, that level will be achieved in a timescale of a few nonlinear turnover times. It would be desirable to develop a quantitative theoretical understanding of that favored level of parallel variance for turbulent compressible MHD as a function of the turbulence parameters. This is deferred to future work.

Acknowledgments
This research is supported in part by NSF AGS-1063439 and AGS-1156094 (SHINE) and by NASA grants NNX15AB88G (LWS) and NNX14AI63G (Heliophysics Grand Challenges) and the Solar Probe Plus project under subcontract D99031L from the Southwest Research Institute ISOIS project and a subcontract from Space Science Institute on NSF grant AGS-1460130. Access to the simulation data used to produce the table and figures, and inform the analysis in the paper, can be provided upon request.

References

Barnes, A. (1979), Hydromagnetic waves and turbulence in the solar wind, in *Solar System Plasma Physics*, vol. 1, edited by E. N. Parker, C. F. Kennel, and L. J. Lanzerotti, pp. 249–319, North-Holland Publishing Co., Amsterdam.

Barnes, A., and J. V. Hollweg (1974), Large-amplitude hydromagnetic waves, *J. Geophys. Res.*, *79*, 2302–2318, doi:10.1029/JA079i016p02302.

Batchelor, G. K. (1970), *The Theory of Homogeneous Turbulence*, Cambridge Univ. Press, Cambridge, U. K.

Bavassano, B., M. Dobrowolny, F. Mariani, and N. F. Ness (1982), Radial evolution of power spectra of interplanetary Alfvénic turbulence, *J. Geophys. Res.*, *87*, 3617–3622, doi:10.1029/JA087iA05p03617.

Belcher, J. W., and L. Davis Jr. (1971), Large-amplitude Alfvén waves in the interplanetary medium. 2, *J. Geophys. Res.*, *76*, 3534–3563, doi:10.1029/JA076i016p03534.

Bieber, J. W., W. Wanner, and W. H. Matthaeus (1996), Dominant two-dimensional solar wind turbulence with implications for cosmic ray transport, *J. Geophys. Res.*, *101*, 2511–2522, doi:10.1029/95JA02588.
Bigot, B., and S. Galtier (2011), Two-dimensional state in driven magnetohydrodynamic turbulence, *Phys. Rev. E*, *83*, 26405, doi:10.1103/PhysRevE.83.026405.
Bigot, B., S. Galtier, and H. Politano (2008), Development of anisotropy in incompressible magnetohydrodynamic turbulence, *Phys. Rev. E*, *78*, 66301, doi:10.1103/PhysRevE.78.066301.
Bruno, R., and V. Carbone (2013), The solar wind as a turbulence laboratory, *Living Rev. Sol. Phys.*, *10*(2), doi:10.12942/lrsp-2013-2.
Bruno, R., B. Bavassano, E. Pietropaolo, V. Carbone, and P. Veltri (1999), Effects of intermittency on interplanetary velocity and magnetic field fluctuations anisotropy, *Geophys. Res. Lett.*, *26*, 3185–3188, doi:10.1029/1999GL010668.
Canuto, C., M. Y. Hussaini, A. Quarteroni, and T. A. Zang (1988), *Spectral Methods in Fluid Mechanics*, Springer-Verlag, New York.
Cho, J., and A. Lazarian (2002), Compressible sub-Alfvénic MHD turbulence in low-β plasmas, *Phys. Rev. Lett.*, *88*, 245001, doi:10.1103/PhysRevlett88.245001.
Cho, J., and A. Lazarian (2003), Compressible magnetohydrodynamic turbulence: Mode coupling, scaling relations, anisotropy, viscosity-damped regime and astrophysical implications, *Mon. Not. R. Astron. Soc.*, *345*, 325–339, doi:10.1046/j.1365-8711.2003.06941.x.
Coleman, P. J. (1968), Turbulence, viscosity, and dissipation in the solar wind plasma, *Astrophys. J.*, *153*, 371–388, doi:10.1086/149674.
Craya, A. (1958), *Contribution à L'Analyse de la Turbulence Associée à des Vitesses Moyennes*, Publ. Sci. Tech. Ministère de l'Air, no. 345, Paris.
Dong, Y., A. Verdini, and R. Grappin (2014), Evolution of turbulence in the expanding solar wind: A numerical study, *Astrophys. J.*, *793*, 118, doi:10.1088/0004-637X/793/2/118.
Ghosh, S., and W. H. Matthaeus (1992), Low Mach number two-dimensional hydrodynamic turbulence: Energy budgets and density fluctuations in a polytropic fluid, *Phys. Fluids A*, *4*, 148, doi:10.1063/1.858492.
Ghosh, S., M. Hossain, and W. H. Matthaeus (1993), The application of spectral methods in simulating compressible fluid and magnetofluid turbulence, *Comput. Phys. Commun.*, *74*, 18–40, doi:10.1016/0010-4655(93)90103-J.
Ghosh, S., W. H. Matthaeus, D. A. Roberts, and M. L. Goldstein (1998a), The evolution of slab fluctuations in the presence of pressure balanced structures and velocity shears, *J. Geophys. Res.*, *103*, 23,691–23,704, doi:10.1029/98JA02195.
Ghosh, S., W. H. Matthaeus, D. A. Roberts, and M. L. Goldstein (1998b), Waves, structures, and the appearance of two-component turbulence in the solar wind, *J. Geophys. Res.*, *103*, 23705–23715, doi:10.1029/98JA02194.
Goldreich, P., and S. Sridhar (1995), Toward a theory of interstellar turbulence: II. Strong Alfvénic turbulence, *Astrophys. J.*, *438*, 763–775, doi:10.1086/175121.
Goldreich, P., and S. Sridhar (1997), Magnetohydrodynamic turbulence revisited, *Astrophys. J.*, *485*, 680–688, doi:10.1086/304442.
Grappin, R., and M. Velli (1996), Waves and streams in the expanding solar wind, *J. Geophys. Res.*, *101*, 425–444, doi:10.1029/95JA02147.
Grappin, R., W.-C. Müller, and A. Verdini (2016), Alfvén-dynamo balance and magnetic excess in MHD turbulence, *Astron. Astrophys.*, *589*, A131, doi:10.1051/0004-6361/201628097.
Hamilton, K., C. W. Smith, B. J. Vasquez, and R. J. Leamon (2008), Anisotropies and helicities in the solar wind inertial and dissipation ranges at 1 AU, *J. Geophys. Res.*, *113*, A01106, doi:10.1029/2007JA012559.
Herring, J. R. (1974), Approach of axisymmetric turbulence to isotropy, *Phys. Fluids*, *17*, 859–872, doi:10.1063/1.1694822.
Horbury, T., A. Balogh, R. J. Forsyth, and E. J. Smith (1995), Ulysses magnetic field observations of fluctuations within polar coronal flows, *Ann. Geophys.*, *13*, 105–107.
Howes, G. G. (2015), The inherently three-dimensional nature of magnetized plasma turbulence, *J. Plasma Phys.*, *81*, 325810203, doi:10.1017/S0022377814001056.
Howes, G. G., and K. D. Nielson (2013), Alfvén wave collisions, the fundamental building block of plasma turbulence: I. Asymptotic solution, *Phys. Plasmas*, *20*, 72302, doi:10.1063/1.4812805.
Howes, G. G., S. D. Bale, K. G. Klein, C. H. K. Chen, C. S. Salem, and J. M. TenBarge (2012), The slow-mode nature of compressible wave power in solar wind turbulence, *Astrophys. J.*, *753*, L19, doi:10.1088/2041-8205/753/1/L19.
Kadomtsev, B. B., and O. P. Pogutse (1974), Nonlinear helical perturbations of a plasma in the tokamak, *Sov. Phys.–J. Exp. Theor. Phys.*, *38*, 283–290, [Zh. Eksp. Teor. Fiz. 65, 575 (1973)].
Klein, K. G., G. G. Howes, J. M. TenBarge, S. D. Bale, C. H. K. Chen, and C. S. Salem (2012), Using synthetic spacecraft data to interpret compressible fluctuations in solar wind turbulence, *Astrophys. J.*, *755*, 159, doi:10.1088/0004-637X/755/2/159.
Klein, L. W., D. A. Roberts, and M. L. Goldstein (1991), Anisotropy and minimum variance directions of solar wind fluctuations in the outer heliosphere, *J. Geophys. Res.*, *96*, 3779–3788, doi:10.1029/90JA02240.
Klein, L. W., R. Bruno, B. Bavassano, and H. Rosenbauer (1993), Anisotropy and minimum variance directions of magnetohydrodynamic fluctuations in the inner heliosphere, *J. Geophys. Res.*, *98*, 17,461–17,466, doi:10.1029/93JA01522.
Leamon, R. J., C. W. Smith, N. F. Ness, W. H. Matthaeus, and H. K. Wong (1998), Observational constraints on the dynamics of the interplanetary magnetic field dissipation range, *J. Geophys. Res.*, *103*, 4775, doi:10.1029/97JA03394.
Lee, J. (1975), The triad-interaction representation of homogeneous turbulence, *J. Math. Phys.*, *16*, 1359–1366, doi:10.1063/1.522704.
Lesieur, M. (1990), *Turbulence in Fluids*, Kluwer, 2nd ed., Dordrecht, Netherlands.
Lighthill, M. J. (1952), On sound generated aerodynamically, *Proc. R. Soc. A*, *211*, 564–587, doi:10.1098/rspa.1952.0060.
Lithwick, Y., and P. Goldreich (2001), Compressible magnetohydrodynamic turbulence in interstellar plasmas, *Astrophys. J.*, *562*, 279–296, doi:10.1086/323470.
MacBride, B. T., C. W. Smith, and M. A. Forman (2008), The turbulent cascade at 1 AU: Energy transfer and the third-order scaling for MHD, *Astrophys. J.*, *679*, 1644–1660, doi:10.1086/529575.
MacBride, B. T., C. W. Smith, and B. J. Vasquez (2010), Inertial-range anisotropies in the solar wind from 0.3 to 1 AU: Helios 1 observations, *J. Geophys. Res.*, *115*, A07105, doi:10.1029/2009JA014939.
Marino, R., L. Sorriso-Valvo, V. Carbone, A. Noullez, R. Bruno, and B. Bavassano (2008), Heating the solar wind by a magnetohydrodynamic turbulent energy cascade, *Astrophys. J.*, *677*, L71–L74, doi:10.1086/587957.
Marino, R., L. Sorriso-Valvo, V. Carbone, P. Veltri, A. Noullez, and R. Bruno (2011), The magnetohydrodynamic turbulent cascade in the ecliptic solar wind: Study of Ulysses data, *Planet. Space Sci.*, *59*, 592–597, doi:10.1016/j.pss.2010.06.005.
Matthaeus, W. H., and M. L. Goldstein (1982), Measurement of the rugged invariants of magnetohydrodynamic turbulence in the solar wind, *J. Geophys. Res.*, *87*, 6011–6028, doi:10.1029/JA087iA08p06011.
Matthaeus, W. H., and S. L. Lamkin (1986), Turbulent magnetic reconnection, *Phys. Fluids*, *29*, 2513–2534, doi:10.1063/1.866004.
Matthaeus, W. H., S. Ghosh, S. Oughton, and D. A. Roberts (1996), Anisotropic three-dimensional MHD turbulence, *J. Geophys. Res.*, *101*, 7619–7629, doi:10.1029/95JA03830.
Montgomery, D., and L. Turner (1982), Two-and-a-half-dimensional magnetohydrodynamic turbulence, *Phys. Fluids*, *25*, 345–349, doi:10.1063/1.863741.

Montgomery, D. C. (1982), Major disruption, inverse cascades, and the Strauss equations, *Phys. Scr.*, *T2/1*, 83–88, doi:10.1088/0031-8949/1982/T2A/009.
Montgomery, D. C., M. R. Brown, and W. H. Matthaeus (1987), Density fluctuation spectra in MHD turbulence, *J. Geophys. Res.*, *92*, 282–284, doi:10.1029/JA092iA01p00282.
Nielson, K. D., G. G. Howes, and W. Dorland (2013), Alfvén wave collisions, the fundamental building block of plasma turbulence: II. Numerical solution, *Phys. Plasmas*, *20*, 72303, doi:10.1063/1.4812807.
Osman, K. T., M. Wan, W. H. Matthaeus, B. Breech, and S. Oughton (2011a), Directional alignment and non-Gaussian statistics in solar wind turbulence, *Astrophys. J.*, *741*, 75, doi:10.1088/0004-637X/741/2/75.
Osman, K. T., M. Wan, W. H. Matthaeus, J. M. Weygand, and S. Dasso (2011b), Anisotropic third-moment estimates of the energy cascade in solar wind turbulence using multispacecraft data, *Phys. Rev. Lett.*, *107*, 165001, doi:10.1103/PhysRevLett.107.165001.
Oughton, S., E. R. Priest, and W. H. Matthaeus (1994), The influence of a mean magnetic field on three-dimensional MHD turbulence, *J. Fluid Mech.*, *280*, 95–117, doi:10.1017/S0022112094002867.
Oughton, S., K.-H. Rädler, and W. H. Matthaeus (1997), General second-rank correlation tensors for homogeneous magnetohydrodynamic turbulence, *Phys. Rev. E*, *56*, 2875–2888, doi:10.1103/PhysRevE.56.2875.
Oughton, S., W. H. Matthaeus, M. Wan, and K. T. Osman (2015), Anisotropy in solar wind plasma turbulence, *Philos. Trans. R. Soc. A*, *373*, 20140152, doi:10.1098/rsta.2014.0152.
Parashar, T. N., W. H. Matthaeus, M. Wan, and S. Oughton (2016), Variance anisotropy in kinetic plasmas, *Astrophys. J.*, *824*(1), 44.
Passot, T., and A. Pouquet (1987), Numerical simulation of compressible flows in the turbulent regime, *J. Fluid Mech.*, *181*, 441–466, doi:10.1017/S0022112087002167.
Perri, S., and A. Balogh (2010), Differences in solar wind cross-helicity and residual energy during the last two solar minima, *Geophys. Res. Lett.*, *37*, L17102, doi:10.1029/2010GL044570.
Pouquet, A., U. Frisch, and J. Léorat (1976), Strong MHD helical turbulence and the nonlinear dynamo effect, *J. Fluid Mech.*, *77*, 321–354, doi:10.1017/S0022112076002140.
Roberts, D. A. (2010), Evolution of the spectrum of solar wind velocity fluctuations from 0.3 to 5 AU, *J. Geophys. Res.*, *115*, A12101, doi:10.1029/2009JA015120.
Roberts, D. A., L. W. Klein, M. L. Goldstein, and W. H. Matthaeus (1987a), The nature and evolution of magnetohydrodynamic fluctuations in the solar wind: Voyager observations, *J. Geophys. Res.*, *92*, 11,021–11,040, doi:10.1029/JA092iA10p11021.
Roberts, D. A., M. L. Goldstein, L. W. Klein, and W. H. Matthaeus (1987b), Origin and evolution of fluctuations in the solar wind: Helios observations and Helios-Voyager comparisons, *J. Geophys. Res.*, *92*, 12023–12035, doi:10.1029/JA092iA11p12023.
Robinson, D. C., and M. G. Rusbridge (1971), Structure of turbulence in the zeta plasma, *Phys. Fluids*, *14*, 2499–2511, doi:10.1063/1.1693359.
Schekochihin, A. A., S. C. Cowley, W. Dorland, G. W. Hammett, G. G. Howes, E. Quataert, and T. Tatsuno (2009), Astrophysical gyrokinetics: Kinetic and fluid turbulent cascades in magnetized weakly collisional plasmas, *Astrophys. J. Suppl. Ser.*, *182*, 310–377, doi:10.1088/0067-0049/182/1/310.
Shebalin, J. V., W. H. Matthaeus, and D. Montgomery (1983), Anisotropy in MHD turbulence due to a mean magnetic field, *J. Plasma Phys.*, *29*, 525–547, doi:10.1017/S0022377800000933.
Smith, C. W., B. J. Vasquez, and K. Hamilton (2006), Interplanetary magnetic fluctuation anisotropy in the inertial range, *J. Geophys. Res.*, *111*, A09111, doi:10.1029/2006JA011651.
Sorriso-Valvo, L., R. Marino, V. Carbone, A. Noullez, F. Lepreti, P. Veltri, R. Bruno, B. Bavassano, and E. Pietropaolo (2007), Observation of inertial energy cascade in interplanetary space plasma, *Phys. Rev. Lett.*, *99*, 115001, doi:10.1103/PhysRevLett.99.115001.
Sridhar, S., and P. Goldreich (1994), Toward a theory of interstellar turbulence: I. Weak Alfvénic turbulence, *Astrophys. J.*, *432*, 612–621, doi:10.1086/174600.
Stawarz, J. E., C. W. Smith, B. J. Vasquez, M. A. Forman, and B. T. MacBride (2009), The turbulent cascade and proton heating in the solar wind at 1 AU, *Astrophys. J.*, *697*, 1119–1127, doi:10.1088/0004-637X/697/2/1119.
Stawarz, J. E., C. W. Smith, B. J. Vasquez, M. A. Forman, and B. T. MacBride (2010), The turbulent cascade for high cross-helicity states at 1 AU, *Astrophys. J.*, *713*, 920–934, doi:10.1088/0004-637X/713/2/920.
Strauss, H. R. (1976), Nonlinear, three-dimensional magnetohydrodynamics of noncircular tokamaks, *Phys. Fluids*, *19*, 134–140, doi:10.1063/1.861310.
Tu, C.-Y., and E. Marsch (1995), MHD structures, waves and turbulence in the solar wind, *Space Sci. Rev.*, *73*, 1–210, doi:10.1007/BF00748891.
Velli, M., R. Grappin, and A. Mangeney (1989), Turbulent cascade of incompressible unidirectional Alfvén waves in the interplanetary medium, *Phys. Rev. Lett.*, *63*, 1807–1810, doi:10.1103/PhysRevLett.63.1807.
Verdini, A., and R. Grappin (2015), Imprints of expansion on the local anisotropy of solar wind turbulence, *Astrophys. J.*, *808*, L34, doi:10.1088/2041-8205/808/2/L34.
Verdini, A., R. Grappin, P. Hellinger, S. Landi, and W. C. Müller (2015), Anisotropy of third-order structure functions in MHD turbulence, *Astrophys. J.*, *804*, 119, doi:10.1088/0004-637X/804/2/119.
Völk, H. J., and W. Aplers (1973), The propagation of Alfvén waves and their directional anisotropy in the solar wind, *Astrophys. Space Sci.*, *20*, 267–285, doi:10.1007/BF00642204.
Wan, M., K. T. Osman, W. H. Matthaeus, and S. Oughton (2012), Investigation of intermittency in magnetohydrodynamics and solar wind turbulence: Scale-dependent kurtosis, *Astrophys. J.*, *744*, 171, doi:10.1088/0004-637X/744/2/171.
Yokoi, N. (2011), Modeling the turbulent cross-helicity evolution: Production, dissipation, and transport rates, *J. Turb.*, *12*, N27, doi:10.1080/14685248.2011.590495.
Zank, G. P., and W. H. Matthaeus (1992), The equations of reduced magnetohydrodynamics, *J. Plasma Phys.*, *48*, 85–100, doi:10.1017/S002237780001638X.
Zank, G. P., and W. H. Matthaeus (1993), Nearly incompressible fluids. II: Magnetohydrodynamics, turbulence, and waves, *Phys. Fluids A*, *5*, 257–273, doi:10.1063/1.858780.
Zhou, Y., and W. H. Matthaeus (1989), Non-WKB evolution of solar wind fluctuations: A turbulence modeling approach, *Geophys. Res. Lett.*, *16*, 755–758, doi:10.1029/GL016i007p00755.